Eur. Phys. J. B **23**, 171–178 (2001)

THE EUROPEAN PHYSICAL JOURNAL B

EDP Sciences

Density dependence of mean kinetic energy in liquid and solid hydrogen at 19.3 K

M. Zoppi[1,a], D. Colognesi[2], and M. Celli[1]

[1] Consiglio Nazionale delle Ricerche, Istituto di Elettronica Quantistica, Via Panciatichi 56/30, 50127 Firenze, Italy
[2] Consiglio Nazionale delle Ricerche, Gruppo Nazionale di Struttura della Materia, Viale dell'Università 11, 00185 Roma, Italy

Received 8 February 2001 and Received in final form 24 April 2001

Abstract. We have measured, using the TOSCA spectrometer at ISIS, the inelastic incoherent neutron scattering spectrum of liquid and solid para-hydrogen along the $T = 19.3$ K isotherm. From the high-energy region of the spectrum, where the Impulse Approximation for the Centre of Mass motion applies, we have been able to extract the mean translational kinetic energy, which, as expected, turns out rather different from the classical value and density dependent. We find that the density behaviours in the liquid and the solid phase are slightly different. This confirms a similar feature already observed in liquid and solid helium at $T = 6.1$ K [M. Celli, M. Zoppi, J. Mayers, Phys. Rev. B **58**, 242 (1998)]. The spectra from the solid phase have been also analysed in the low-energy region and allowed us to derive the Debye-Waller factor of solid para-hydrogen as a function of density. The comparison with the available experimental data in the literature is rather good and confirms the excellent performances of TOSCA in the spectroscopic analysis of the condensed phases of para-hydrogen.

PACS. 61.12.Ex Neutron scattering techniques (including small-angle scattering) – 64.70.Dv Solid-liquid transitions – 67.90.+z Other topics in quantum fluids and solids; liquid and solid helium

1 Introduction

The dynamics of simple systems can be directly accessed by means of Inelastic Neutron Scattering (INS) [1]. The double differential cross section for INS is given by [2]:

$$\frac{\mathrm{d}^2\sigma}{\mathrm{d}\Omega\mathrm{d}\omega} = \frac{k_1}{k_0}\frac{1}{2\pi\hbar}\sum_{i,j} b_i b_j \int_{-\infty}^{+\infty} \mathrm{d}t \exp(-\mathrm{i}\omega t) \times \langle \exp\left[-\mathrm{i}\mathbf{k}\cdot\mathbf{R}_i(0)\right] \exp\left[\mathrm{i}\mathbf{k}\cdot\mathbf{R}_j(t)\right]\rangle , \quad (1)$$

where: $\mathrm{d}\Omega$ is the collection solid angle, k_0 and k_1 are the incident and scattered neutron wavevectors, b_i is the scattering length of the ith nucleus, $\hbar\mathbf{k} = \hbar\mathbf{k}_0 - \hbar\mathbf{k}_1$ is the momentum transfer, and $\hbar\omega = E_0 - E_1$ is the energy transfer. The sum over i and j extends over the nuclei contained in the scattering volume and the angular brackets mean (quantum) thermodynamic average over the sample.

The time dependent pair correlation function $F_{i,j}(\mathbf{k},t)$, defined as:

$$F_{i,j}(\mathbf{k},t) = \langle \exp\left[-\mathrm{i}\mathbf{k}\cdot\mathbf{R}_i(0)\right] \exp\left[\mathrm{i}\mathbf{k}\cdot\mathbf{R}_j(t)\right]\rangle , \quad (2)$$

contains all the relevant dynamic information. This represents the joint probability that the particle j can be found in the position $\mathbf{R}_j$, at time t, given that the particle i, which can be the same or a different one, is found at $t = 0$ in the position $\mathbf{R}_i$. Thus, $F_{i,j}(\mathbf{k},t)$ contains all the dynamic information relative to the average motion of a single particle with respect to its initial position (*self* term) or the relative motion of a particle with respect to another one (*distinct* term). The system dynamics is determined by its Hamiltonian operator, which includes all the interactions among the particles of the sample.

INS experiments are usually carried out in different regions of momentum, $\hbar k$, and energy transfer, $\hbar\omega$, depending on the particular neutron spectrometer. It is well known that, by changing the (k,ω) range, different dynamic regimes are sampled. In the low-k region ($0 < k < 5{-}10$ Å^{-1}) the collective properties of a molecular sample are probed. In this region, the dynamics is mainly determined by the inter-molecular correlations. The intermediate-k region ($5{-}10$ Å$^{-1} < k < 20{-}30$ Å^{-1}) is related to the intra-molecular interactions. Here, the molecular structure and internal force-constants mainly determine the molecular dynamics, which, in turn, becomes almost independent of the motion of the neighbouring molecules. As the momentum transfer further increases (in practice when $k > 30$ Å^{-1}) we enter the so-called *Impulse Approximation* (IA) regime where the scattering function becomes insensitive to the atomic interactions and depends only on the initial conditions of the system. In the validity range of the IA regime, the scattering function reduces to a recoil peak whose shape

[a] e-mail: zoppi@ieq.fi.cnr.it

is only determined by the momentum distribution of the target atoms [3].

For classical systems, the momentum distribution of the molecular translational motion is determined by the Maxwell-Boltzmann velocity distribution. This is a three-dimensional Gaussian function whose width is related to the average translational kinetic energy which, in turn, is given by the temperature according to the usual relation: $\langle E_k \rangle = \frac{3}{2} k_{\mathrm{B}} T$. As quantum effects become relevant, both the shape and the width of the momentum distribution can change and values for the kinetic energy different from the classical limit can be observed. These effects usually appear at low temperature, as in the case of quantum liquids, but can also manifest at relatively high temperature, as in the case of solids with a high Debye temperature. At any rate, any deviation from the classical behaviour of the momentum distribution is a clear signature of the emergence of quantum effects.

Deep inelastic neutron scattering, also known as *Neutron Compton Scattering* (NCS) [4], is an experimental technique that makes use of the epithermal neutrons, produced by a Spallation Neutron Source, to probe materials in a regime of very high momentum and energy transfer, *i.e.* within the limits of applicability of the IA. By means of NCS one can access direct information on the momentum distribution of atomic particles at the microscopic level. In particular, this technique has been used, in the recent years, to measure the behaviour of the mean kinetic energy in low temperature normal liquid and solid ^{4}He as a function of the thermodynamic state [5–12].

The density and temperature behaviours of mean kinetic energy in a quantum system are still matter of research. For the temperature dependence, at constant density, data are usually well represented both by an Einstein oscillator and an effective Debye model [6]. These two models merge into the classical behaviour at sufficiently high temperature. For the density dependence, it has been suggested that the changes in mean kinetic energy are produced by variations in the excluded volume [7,8,11]. As the volume available to an atomic particle becomes smaller and smaller, then, because of the Heisenberg's uncertainty principle, the variance of the single particle momentum increases and so does its mean kinetic energy. This simplified representation of reality has the advantage of being intuitive and qualitatively correct.

The first experimental determinations [13] of the mean kinetic energy of liquid and solid hydrogen were rather uncertain (∼10%). Following determinations, in the solid phase [14], were more accurate (4–11%), and a linear fit in $1/n$, where n is the number density, was suggested. The same experimental data were also compared with the Path Integral Monte Carlo (PIMC) simulation results [15] and a rough density dependence with n^2 was suggested, mostly based on the simulation results. This functional form had the advantage of being simple but no theoretical explanation was developed at the time, and it was somehow justified by the relatively small density interval where the density analysis was carried out.

In recent NCS experiments [8,11], the kinetic energy of liquid and solid helium has been measured at low temperature along a supercritical isotherm. In this way, a large density interval could be explored, between 6 nm^{-3} and the freezing point (35 nm^{-3}), and the density behaviour over a much larger range of the fluid phase could be obtained. This was fitted by a power-law function:

$$\langle E_k \rangle = \frac{3}{2} k_{\mathrm{B}} T + A n^P, \tag{3}$$

where $P = 2.46$. No theoretical explanation exists for this functional form, which should be only considered as a useful parametric representation. The NCS experiment was also extended to the solid phase. However, it turned out that the extrapolation to the solid phase, of the same functional form determined in the liquid, produced a different density behaviour than that actually measured (see Fig. 2 of Ref. [11]). This fact is in contrast with the hypothesis of a simple excluded volume effect to explain the density evolution of the kinetic energy and suggests that a more detailed structural information may have some role. On the other hand, it should be pointed out that other authors found different results and draw dissimilar conclusions [9,12].

In order to shed some light on this interesting aspect of the problem, we thought that more experimental results would be necessary. An obvious extension could have been to run an independent experiment on the same system, namely helium, but along a different isotherm. However, we thought that more convincing results could be obtained by changing the nature of the quantum system. Molecular hydrogen, therefore, was the obvious choice. In fact, even though the freezing temperature of liquid hydrogen is rather large, compared to helium, its molecular mass is smaller and therefore the hydrogen quantum features are rather large and comparable with those of normal helium.

Measuring the mean kinetic energy of molecular hydrogen by using the same neutron instrument that was used for the helium experiment, namely the electron volt spectrometer eVS, does not allow the required precision [16]. In fact, the range of momentum transfer that is tested on eVS is so large (>30 Å^{-1}) that one measures directly the kinetic energy of the protons in the hydrogen molecule [17]. As the rotational and vibrational components of the molecular energy add to the translational component of the molecular kinetic energy, such a measurement would have been intrinsically less precise than it was needed. In practice, the experimental problem reduces to the fact that we want to have a momentum transfer high enough that the IA can be applied for the *centre-of-mass* (CoM) motion of the molecule. On the other hand, the energy-momentum transfer should be small enough that the molecular character of hydrogen is not disrupted by the experiment (the intra-molecular final state must still be a bound state of the molecule). Therefore eVS had to be excluded.

We have recently shown that an instrument satisfying the above requirements exists. The TOSCA spectrometer, recently built at ISIS [18], has the necessary characteristics. Using this instrument we have shown that the

translational kinetic energy of the CoM of molecular para-hydrogen can be measured [19] with a precision that sensibly improves the previous determinations [13,14,20].

In this paper we report the results of an experiment, carried out on liquid and solid para-hydrogen, aiming to the measurement of the translational mean kinetic energy of the molecular centre-of-mass as a function of density. The experiment has been carried out on the isotherm at $T = (19.3 \pm 0.1)$ K. In Section 2 we will describe the details of the experiment. Section 3 is devoted to the analysis of the experimental data and the derivation of the mean kinetic energy values. In Section 4 we discuss further results obtained from the experiment, and the conclusions are drawn in Section 5.

Table 1. Thermodynamic data and experimental measurement time (I.C. = integrated proton current). The numbers in brackets are standard deviations and affect the last significant digit.

T (K)	p (bar)	n (nm^{-3})	Phase	I.C. (μAh)
19.33(1)	17.4(5)	22.04(1)	Liq.	664.3
19.36(2)	90.9(5)	23.83(1)	Liq.	3566.6
19.34(2)	191(2)	25.43(3)	Liq.	3065.8
19.34(2)	395(2)	29.56(1)	Sol.	2952.9
19.37(7)	543(2)	30.60(1)	Sol.	3368.3
19.40(1)	636(1)	31.29(1)	Sol.	3791.0
34.99(5)	0.0	empty	-	982.2

2 Experiment details

The measurement was carried out at six thermodynamic points (see Tab. 1). The first three points refer to the liquid, while the three high-density points refer to the solid phase. Of the latter, the one at low density is presumably in the fcc lattice phase while the two at the highest densities should be hcp [21]. However, both the existence of a high temperature fcc phase in para-hydrogen, and the location of its boundary line, are still controversial [22,23]. At any rate, we believe that this interesting problem has almost no impact on the present study, devoted to single particle properties, since the first three shells of nearest neighbours are identical for the two cases [24].

After performing the background measurements of the empty cryostat, we cooled the scattering cell at the desired temperature ($T = 19.3$ K) and we measured its time-of-flight (TOF) spectrum. Then, hydrogen was allowed to condense in the scattering cell. This was made of SS-316 steel and consisted of an array of 5 tubes (O.D. 3.2 mm, I.D. 1.6 mm), 64.0 mm high and 5.5 mm apart to one another, so as to minimise the multiple scattering contributions. At the bottom of the scattering container, out of the neutron beam, we had inserted some powder of paramagnetic catalyst made of Cr_2O_3 and γ-Al_2O_3 in order to accelerate the transition rate from ortho- to para-hydrogen.

The pressure of the gas handling system was set to $p = 191.2$ bar, a pressure just below the freezing point at this temperature. The relative concentration of the two species was monitored looking at the scattering spectrum. In particular, we could observe the progressive disappearance of the $J = 1 \rightarrow J' = 1$ transition, that is weighted by the incoherent cross section of the proton, from the quasi-elastic portion of the spectrum. When this spectral component was below the limit of detectability (in practice, masked by the $J = 0 \rightarrow J' = 0$ transition, that is weighted by the coherent cross section of the proton) we assumed that the equilibrium was reached. The equilibration process took, in this case, about 24 hours. The estimated concentration of para-hydrogen, based on the theoretical analysis, is assumed to be 99.82%. Then, we started recording the scattering spectrum up to an integrated proton current of 3065.8 μAh (about 18 hours of measurement).

The spectra in the solid phase were taken in a similar way. The set-point temperature of the scattering cell was kept constant and we modified only the pressure. After changing the hydrogen pressure in the gas line, we took care of heating the inlet of the sample cell to make sure that the sample pressure was in equilibrium with the reading of the pressure gauge. The input tube of the scattering cell was then allowed to cool down slowly to the same temperature of the cell body so as to make sure that the inlet hole was the last part where the sample solidified. This procedure implies some transfer from the gas line into the scattering cell. However, this amount of gas is extremely small and is located in the highest part of the scattering cell, which however was kept out of the neutron beam. The absence of the spectral line corresponding to the $J = 1 \rightarrow J' = 1$ transition was checked every run to exclude any unwanted sample contamination from ortho-hydrogen. The three solid phase runs were carried out for comparable amounts of time (see Tab. 1). Each change of pressure was performed as described above.

After completing the solid-state runs, the system was then brought back to the liquid phase. To this aim, after warming the cell inlet, the pressure was gently released, allowing the sample to slowly decrease its density and eventually to melt. The precise melting transition could be observed in the neutron scattering spectrum looking at the disappearance of the sharp rotational line at $\hbar\omega = 14.2$ meV [25]. The system was then brought to the desired pressure in the liquid phase and two more points were measured.

The stability of the thermodynamic conditions during the experiment was very good. The temperature fluctuations never exceeded 0.2 K and the pressure stability was strictly related to this value, thanks to the very good realisation of the gas handling system. The densities of our samples were derived according to reference [21]. The full set of parameters characterising the present experiment is reported in Table 1.

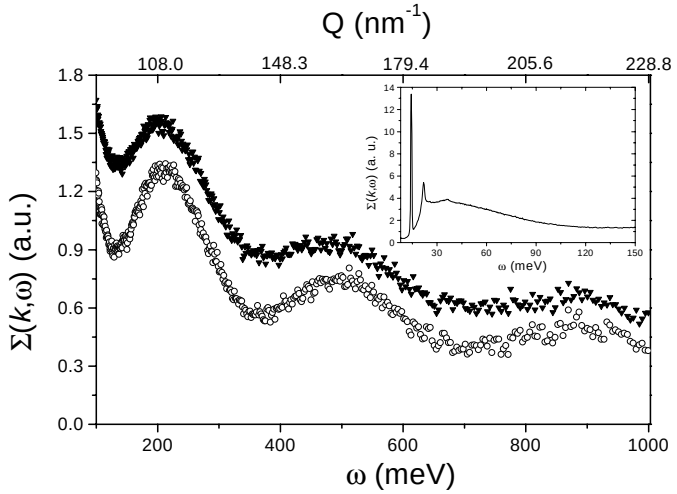

Fig. 1. Inelastic neutron spectra of liquid (open circles: $n = 22.04$ nm^{-3}) and solid (full triangles: $n = 31.29$ nm^{-3}) para-hydrogen from TOSCA. Raw data are shown in the energy range used for the mean kinetic energy fitting procedure (see Sect. 3). The insert shows a typical spectrum of solid para-hydrogen ($n = 31.29$ nm^{-3}) in the low-energy region. The sharp line observed at $\hbar\omega = 14.2$ meV corresponds to the ($J = 0 \rightarrow J' = 1$) rotational transition.

3 Experimental results for the mean kinetic energy

As it was explained in the report of our previous test experiment on TOSCA [19] not all the spectral information can be used to extract the translational kinetic energy. In fact, in the low energy portion of the spectrum (in essence, that extending from $\hbar\omega = 0$ to beyond the first peak of the spectrum) the momentum transfer is not large enough that the IA can be applied to the translational motion and the inter-particle interactions still affect this spectral region [26]. However, starting from just before the first minimum ($\hbar\omega \cong 100$ meV) the value of the momentum transfer becomes large enough ($k > 8$ Å^{-1}) that the IA can be applied to the CoM motion.

In Figure 1, we report two typical raw data spectra of liquid and solid para-hydrogen on TOSCA in the spectral range used to extract the mean kinetic energy. Since the sample is at low temperature, and at a relatively low density, only the $J = 0$ rotational state is populated (at least up to a density of 32 nm^{-3}, see Ref. [27]) and the various broad peaks observed in the figure correspond to the rotational transitions from $J = 0$ to the odd rotational numbers ($J' = 3$, 5, 7). The transitions to the even rotational numbers are also present. However, being weighted by the much smaller coherent cross section of hydrogen, they cannot be seen in the figure. The various peaks are broadened and shifted by the recoil of the CoM and their width contains the requested information on the translational kinetic energy.

If we focus our attention on the rotational transition ($J = 0 \rightarrow J' = n$), where n is an odd integer, the double differential cross section is given by [2,19]:

$$\frac{\mathrm{d}^2\sigma}{\mathrm{d}\Omega\mathrm{d}\omega} = \frac{k_1}{k_0}\frac{\sigma_i}{4\pi}\sum(k,\omega) = \frac{k_1}{k_0}\frac{\sigma_i}{4\pi}|f(k)|^2_{0\rightarrow n} \times S_{\mathrm{self}}(k,\omega) \otimes \delta(\omega - \omega_{0\rightarrow n}) \quad (4)$$

where σ_i is the hydrogen incoherent cross section, $|f(k)|^2_{0\rightarrow n}$ is the intra-molecular form factor of this transition and $S_{\mathrm{self}}(k,\omega)$ is the self, molecular (CoM), dynamic structure factor [2]. The symbol $\otimes$ represents a convolution and δ is the Dirac delta-function. The cross section can be evaluated along the kinematic path of TOSCA [18] to derive a theoretical double differential cross section, provided a suitable model is given for $S_{\mathrm{self}}(k,\omega)$.

In the applicability limit of the IA, the intermediate scattering function, $F_{\mathrm{self}}(k,t)$, *i.e.* the time-Fourier transform of $S_{\mathrm{self}}(k,\omega)$ [2], reduces to:

$$F_{\mathrm{self}}(k,t) \rightarrow F_{\mathrm{IA}}(k,t) = \exp\left\{\mathrm{i}\frac{E_r}{\hbar}t\right\}\langle\exp\{\mathrm{i}\mathbf{k}\cdot\mathbf{v}t\}\rangle \quad (5)$$

where $E_r = \hbar^2k^2/2M$ is the recoil energy, M is the molecular mass, and $\mathbf{v} \equiv \mathbf{v}(0)$ is the velocity of the target particle at time $t = 0$. Within the IA, the dynamics of the molecular CoM is approximated by the ideal-gas model and therefore the dynamic structure factor simply becomes:

$$S_{\mathrm{self}}(k,\omega) = \hbar\int \mathrm{d}\mathbf{p}\, n(\mathbf{p})\,\delta(\hbar\omega - E_r - \hbar\,\mathbf{k}\cdot\mathbf{p}/M), \quad (6)$$

where $\mathbf{p} = M\mathbf{v}$ is the momentum of the target particle and $n(\mathbf{p})$ is its momentum distribution [2,28].

By assuming a known shape for the momentum distribution, namely a Gaussian distribution whose width is determined by the average translational kinetic energy of the molecular CoM, a theoretical cross section can be derived where the only free parameter is the width of the momentum distribution. This allows us to derive a theoretical expression for the measured neutron cross-section using two fitting parameters, namely the translational kinetic energy of the molecular CoM, and an overall normalisation constant.

The six spectra, taken at the various thermodynamic conditions listed in Table 1, have been fitted using equation (4) and their respective translational kinetic energy values have been obtained. These are listed in Table 2 (3rd column). In the first row of Table 2 we have also reported the value of the mean kinetic energy, at the same temperature of the present determination, obtained in our previous experiment [19]. For the details of the data analysis we address the reader to our previous work on low-density liquid para-hydrogen [19]. The kinetic energy data of para-hydrogen, at constant temperature $T = 19.3$ K, are plotted in Figure 2 as a function of density (open circles with error bars). The two vertical (dashed) lines represent the boundaries for the liquid and the solid phase at the same temperature [21]. The lowest density point reported in the figure is relative to our previous experiment [19]. We notice that the statistical accuracy of the present experimental

Table 2. Mean kinetic energy data (experiment and PIMC simulations) and experimental molecular mean square displacements (solid phase only, see text). The numbers in brackets are standard deviations and affect the last significant digit. In the first line, we have included the results of a previous experiment [19].

T (K)	n (nm^{-3})	$\langle E_k\rangle_{\rm exp}$ (K)	$\langle E_k\rangle_{\rm PIMC}$ (K)	$\langle \mathbf{u}^2\rangle$ (Å^2)	$\langle \mathbf{u}^2\rangle_0$ (Å^2)
19.2(2)	21.50(6)	62(1)	61.4(1)	-	-
19.33(1)	22.04(1)	63(3)	62.6(3)	-	-
19.36(2)	23.83(1)	68(3)	68.6(3)	-	-
19.34(2)	25.43(3)	74(5)	74.5(1)	-	-
19.34(2)	29.56(1)	89(4)	90.9(7)	0.47(2)	0.41(2)
19.37(7)	30.60(1)	97(5)	96.6(3)	0.39(2)	0.35(2)
19.40(1)	31.29(1)	102(5)	100.3(8)	0.37(2)	0.33(2)

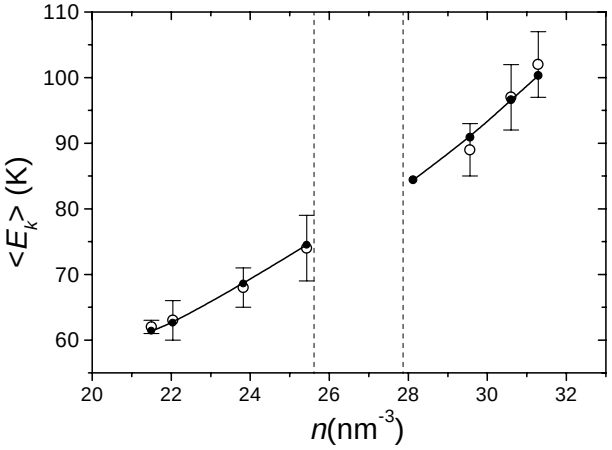

Fig. 2. Density behaviour of mean translational kinetic energy in liquid and solid para-hydrogen at $T = 19.3$ K. Open circles (with error bars) stand for the results derived from the present neutron scattering spectra (*cf.* Tab. 2). Full dots are obtained from PIMC quantum simulations (statistical errors are smaller than the symbol size, full line is an eye-guide). Vertical dashed lines mark the boundaries of the liquid and solid phases.

points is lower than the previous ones. This is related to the smaller scattering volume of the sample, in the present experiment, that was imposed by the use of a high pressure container.

4 PIMC simulation

The computer simulations of liquid and solid para-hydrogen were carried out using the same technique, namely PIMC, which was employed in references [15,19], assuming a pair-wise additive intermolecular potential. For the solid phase, the crystal lattice was considered fcc ($n = 29.56$ nm^{-3}) and hcp ($n = 30.60$ and 31.29 nm^{-3}). Several specific pair potentials are available in the literature and some recent experimental results, using light scattering, suggest that the Schaefer and Köhler potential [29] best represents the low-density experimental results [27]. However, in this case, we preferred to use the semi-empirical model proposed by Silvera and Goldman [30] because it gives a better description of the thermodynamic data of hydrogen in the condensed phases [31].

The number of classical particles was set to $N = 256$ (liquid and fcc), while we have set $N = 180$ for the hcp solid. Although relatively small, the size of N should be sufficient to describe a single particle property like the kinetic energy, which is our main concern here. The particles were assumed to obey the Boltzmann statistics. All interactions were truncated spherically at a cut-off equal to half the minimum edge length of the box, and potential energies and pressures were corrected by integrating over a uniform density beyond the cut-off. The thermodynamic conditions were selected according to the temperature and density of the experimental points (see Tab. 1).

In order to extrapolate the simulation results to the limit $P \to \infty$, we have carried out several simulations by changing the Trotter number P, *i.e.* the number of beads in the ring polymer isomorphic to the quantum particle. In particular, for each thermodynamic point, we used $P = 8$, 16, 32, and 64. The convergence of the results to the quantum mechanical limit was analysed by fitting $\langle E_k\rangle(P)$ as a second order polynomial in $1/P$.

Each simulation was started from a perfect lattice (fcc or hcp) and consisted of 15,000$\times NM$ passes (*i.e.* moves per particle), after a 15,000$\times NM$ passes equilibration stage. Here NM is the *dilution factor*; *i.e.* the number of passes performed before analysing the next configuration. We used $NM = 5$. Thus, averages were accumulated using 15,000 configurations out of each run that, in total, was obtained accumulating $N \times NM \times$ 15,000 Monte Carlo moves (plus equilibration). The results of our simulation are reported in the fourth column of Table 2 and in Figure 2 (full circles). The agreement with the experimental data is excellent. In addition, as there are no experimental data close to the melting line, and with the aim of gaining a better insight of the behaviour of the mean kinetic energy close to the phase transition, a further thermodynamic state has been included in the simulation plans (fcc, $T = 19.34$ K, $n = 28.12$ nm^{-3}) giving rise to: $\langle E_k\rangle = 84.4(2)$ K. This point too is shown in Figure 2.

Thanks to the evident agreement of the simulation results with the experiment, and taking advantage of the better statistical accuracy of PIMC data, we decided to analyse the density behaviour of the mean kinetic energy

using the simulation points. As a first step, we have attempted to describe the density evolution using a simple power law: $\langle E_k \rangle \propto n^P$ for the whole density range (including both liquid and solid phases). However, this function is not able to properly fit our data. On the contrary, individual fitting procedures, applied to liquid and solid phases separately, yield a much better description of the data. Needless to say, the two exponents turn out rather different, $P_{\rm liq} = 1.16(2)$ and $P_{\rm sol} = 1.60(2)$ and, in addition, these values are also different from the one previously found for fluid helium ($P = 2.46$, see Sect. 1).

Of course, one would expect a change in the exponent, even looking at the liquid data only, because of the different interaction potential and the different quantum nature of the two samples (hydrogen and helium). However, we feel that this difference is rather large and we would like to gain a deeper physical insight of the problem. To this aim, we have attempted to subtract from the mean kinetic energy $\langle E_k \rangle$, the purely thermal component in order to obtain the density behaviour of the zero-temperature contribution, namely $\langle E_k \rangle_0 = \langle E_k \rangle (n, T = 0)$. In general, this is rather time-consuming. For example, using PIMC at lower temperatures would imply a substantial increase of the Trotter number, P, with a consequent significant expansion of the CPU time. Moreover, in order to evaluate the $T \to 0$ limit of the kinetic energy, several simulations at different temperatures should be carried out. However, there are two cases where an evaluation of the thermal component is particularly simple. These are the Einstein oscillator model and the Debye model. In addition, the two approximations are very different from each other. Therefore, a comparison between the two results may be enlightening. In both cases, we found, as expected, that the thermal corrections were very similar and much smaller than $\langle E_k \rangle$. Therefore, we could use either one for our purposes. In the end, we decided to use the Debye correction [32]:

$$\langle E_k \rangle = \frac{9}{4} k_{\rm B} T \left(\frac{T}{\Theta_{\rm D}} \right)^3 \int_0^{\Theta_{\rm D}/T} x^3 \coth(x/2) {\rm d}x,$$
$$\langle E_k \rangle_0 = \frac{9}{16} k_{\rm B} \Theta_{\rm D}, \qquad (7)$$

where $\Theta_{\rm D}$ is the effective Debye temperature of the system.

While using the Debye model for a solid-state system is a generally accepted procedure, its extension to the liquid state is not a trivial matter. However, according to the suggestion of reference [33], such an extension seems possible and, to some extent, theoretically justified. At any rate, since the thermal contributions are rather small, we decided to extend the use of the Debye model also to the liquid phase, in order to correct the mean kinetic energy data for the effects of a temperature $T \neq 0$.

As a subsequent step, the data were fitted using a simple Grüneisen law: $\langle E_k \rangle_0 \propto n^\gamma$. This gives rise to the following results: $\gamma_{\rm liq} = 1.30(2)$ and $\gamma_{\rm sol} = 1.67(2)$. It is worthwhile to observe that the latter value is quite similar to $\overline{\gamma}$, the isotropic mean value obtained from the phonon dispersion curves of solid ortho-deuterium between zero pressure and $p = 275$ bar at $T = 5$ K [34]. In fact, using these results we find $\overline{\gamma} = \frac{1}{3}(2\gamma_T + \gamma_L) = 1.63$. On the contrary, the same quantity estimated from the calorimetric data of solid para-hydrogen [35] in the same density and temperature range of the present experiment ($n = 29.11{-}37.19$ nm^{-3} and $T = 18{-}20$ K) gives a value of $\gamma_{\rm sol} = 2.21(5)$. This is not surprising for a non-ideal Debye system, since specific heat is mainly influenced by the low-energy portion of the phonon density of states, while $\langle E_k \rangle_0$ is mostly determined by the high-energy zone.

5 More experimental results in the solid phase

While the liquid phase spectra appear as rather smooth structures dominated by the first rotational transitions shifted and broadened by the CoM recoil, the solid state spectra show some extra features which are mainly concentrated in the low energy region. As observed in the insert of Figure 1, this region is dominated by an intense sharp peak, centered at $\hbar\omega = 14.2$ meV, superimposed to the broad spectral feature common to the two phases. Then, at higher energy, we observe a peak ($\hbar\omega = 21.9$ meV) which has been already interpreted [36] as the maximum of the solid para-hydrogen density of phonon states, shifted by the ($J = 0 \to J' = 1$) rotational transition energy.

The width of the sharp line is instrument resolution-limited (the relative resolution of TOSCA is better than 2% in this spectral region) and could not be measured. We interpret this sharp feature as the ($J = 0 \to J' = 1$) rotational transition for which the CoM recoil is tranferred to the crystal lattice. In the framework of the decoupled model sketched in equation (4), it corresponds to the *elastic contribution* of the solid incoherent structure factor, $S_{\rm self}(k, \omega = 0)$ [2], shifted in energy by an amount fixed by the rotational transition. Thus, we assume that the sharp line (SL) is described by the following cross section:

$$\left[\frac{{\rm d}^2\sigma}{{\rm d}\Omega {\rm d}\omega} \right]_{\rm SL} = \frac{k_1}{k_0} \frac{\sigma_i}{4\pi} |f(k)|^2_{0\to 1} \times \exp\left\{ -2\overline{W}(k) \right\} \delta(\omega - \omega_{0\to 1}) \qquad (8)$$

where $\overline{W}(k)$ is the spherically averaged Debye-Waller factor (our sample is most likely a polycrystal) and the other symbols have the same meaning as in equation (4).

Quantum crystals are generally considered anharmonic [3]. However, in solid hydrogen at various densities, it has been experimentally proven [36,37] that it is possible to express the spherically averaged Debye-Waller factor as: $\overline{W}(k) = \frac{1}{3} k^2 \langle \mathbf{u}^2 \rangle$. This implies an almost Gaussian distribution of the molecular centre of mass around the lattice site and that, at least for k values not larger than 4 Å^{-1}, the higher powers of k in $\overline{W}(k)$ can be neglected. Thus, we can evaluate $\langle \mathbf{u}^2 \rangle$, provided an independent normalisation of the spectra is available. In our case, we used the same normalisation factor that was obtained from the mean kinetic energy fitting procedure applied to

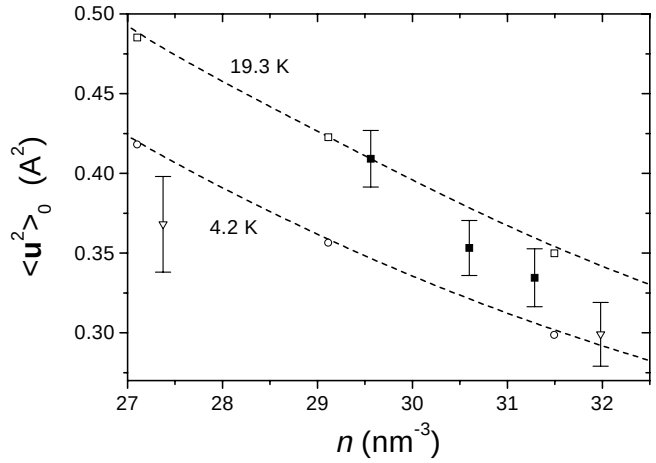

Fig. 3. Density evolution of the zero-temperature mean squared displacement of solid para-hydrogen. Full squares with error bars stand for the results derived from the present neutron scattering spectra at $T = 19.3$ K (sharp line at $\hbar\omega = 14.2$ meV, see insert in Fig. 1). Open triangles with error bars refer to Vindryaevskii's neutron measurements [37] at $T = 4.2$ K. Open squares and circles represent values of $\langle \mathbf{u}^2 \rangle_0$ derived from Krause *et al.* [35] at $T = 19.3$ and $T = 4.2$ K, respectively. Dashed lines are spline fits of the calorimetric data.

the high energy region of the spectra (see Sect. 3). This procedure is, of course, not ideal for evaluating $\langle \mathbf{u}^2 \rangle$, since the normalization constant derived from the Young and Koppel [38] fitting are affected by some uncertainties, of the order of 5% (*e.g.* diffraction measurements would provide more accurate results, both for $\langle \mathbf{u}^2 \rangle$ and n). However, this uncertainty has been correctly propagated in the present determination of the $\langle \mathbf{u}^2 \rangle$ values which are reported in the fifth column of Table 2.

As for the mean kinetic energy, we need to subtract the thermal contribution to compare our results with the available data in the literature. To this aim we used a procedure similar to that described in the previous section and we could obtain the zero-temperature component (density dependent) of the mean square displacement, $\langle \mathbf{u}^2 \rangle_0$. The results are reported in the sixth column of Table 2 and in Figure 3.

We compare, in Figure 3, the present experimental determinations for $\langle \mathbf{u}^2 \rangle_0$ with the data of Vindryaevskii *et al.* [37], also obtained from a neutron scattering experiment, and with those derived by us using the results from calorimetric experiments by Krause and Swenson [35] through the Debye model [32]: $\langle \mathbf{u}^2 \rangle_0 = \frac{9}{4} \frac{\hbar^2}{M k_{\mathrm{B}} \Theta_{\mathrm{D}}}$. It is interesting to observe, that our data are in fair quantitative agreement with the calorimetric determinations at $T = 19.3$ K. On the other hand a similar agreement is found between Vindryaevskii's determinations of $\langle \mathbf{u}^2 \rangle_0$ at $T = 4.2$ K and the Krause's calorimetric ones at the same temperature. This can be easily understood since specific heat is mainly influenced by the low-energy portion of the phonon density of states, likewise $\langle \mathbf{u}^2 \rangle_0$. In addition, the evident temperature variation of $\langle \mathbf{u}^2 \rangle_0$ and Θ_{D} (see for example Refs. [34,35]) which are supposed to depend on density only, is a clear mark of the anharmonicity of solid para-hydrogen.

6 Conclusions

We have reported the density evolution of the translational mean kinetic energy of condensed para-hydrogen as obtained from the inelastic incoherent neutron scattering spectra. Data have been compared with the results a PIMC quantum mechanical simulation and an excellent quantitative agreement has been found. The present data reveal a slightly different density-behaviour between the liquid and the solid phases. Even though the range of densities is not extremely large, the same power law cannot properly describe the density evolution of $\langle E_k \rangle$ in the two phases. Instead, two different exponents are found for the best fits of the data in liquid [$P_{\mathrm{liq}} = 1.16(2)$] and in solid [$P_{\mathrm{sol}} = 1.60(2)$] para-hydrogen. This feature is in qualitative agreement with a similar behaviour already observed in supercritical helium at $T = 6.1$ K [11]; even though the helium exponent for the fluid phase ($P = 2.46$) turns out different from the value of liquid hydrogen. This fact raises an interesting question about a quantitative comparison between these two quantum systems, which should be analysed more thoroughly. However, this is beyond the scope of the present work and will be addressed in a future paper [39].

A useful way to study the problem is to reduce the measured mean kinetic energy to its pure density contribution by subtracting the thermal component. Here we have shown that a simple way of accomplishing this task is to make use of the Debye model, also extended to the liquid state. The main justification for this simple procedure resides in the smallness of the thermal correction itself (see Sect. 4 and Tab. 2). Through this procedure we were able to obtain a zero-temperature evaluation of the mean kinetic energy, $\langle E_k \rangle_0$, which, in turn, was fitted using a simple Grüneisen law: $\langle E_k \rangle_0 \propto n^{\gamma}$. As expected, the value of the Grüneisen parameters for liquid and solid phases, turn out to be different. In addition it is worth mentioning that the value we found for the solid phase of our para-hydrogen sample [$\gamma_{\mathrm{sol}} = 1.67(2)$] is very similar to the isotropic mean of the same quantity ($\overline{\gamma} = 1.63$) obtained from the phonon dispersion curves of low-pressure solid ortho-deuterium (see Sect. 4).

The information content of the solid phase spectra appears richer than the liquid ones. In particular, from the intense sharp peak centered at $\hbar\omega = 14.2$ meV, we were able to obtain the spherically averaged Debye-Waller factor, and from this, the mean square displacement, $\langle \mathbf{u}^2 \rangle$, for solid para-hydrogen at $T = 19.3$ K. Again, by subtracting the thermal contribution (see Sect. 5), we have derived an experimental determination of the zero-temperature component (which is still density-dependent) of the mean square displacement, $\langle \mathbf{u}^2 \rangle_0$. It is interesting to note that our estimate is different from an analogous determination by Vindryaevskii *et al.* [37], also using the neutron scattering technique, but at a quite different temperature

($T = 4.2$ K). On the contrary it is in rather good quantitative agreement with values extracted from data of Krause and Swenson [35], which are based on calorimetric measurements, and interpolated to the same temperature of the present experiment. So we interpret the residual temperature dependence of $\langle \mathbf{u}^2 \rangle_0$ as a clear mark of the solid anharmonicity.

We point out that the observed difference between the Grüneisen parameter for the kinetic energy and that obtained from the specific heat (see Sect. 5), can be seen as direct consequence of the non-Debye nature of the system, *i.e.* the existence of a high-energy tail in the phonon density of states [40]. In fact, both quantities could be calculated integrating over the density of states, $Z(\omega)$, a peculiar energy-weighting function. However, while the specific heat is mainly influenced by the low-energy region of $Z(\omega)$, which incidentally also determines the value of $\langle \mathbf{u}^2 \rangle_0$, the mean kinetic energy is mainly determined by the high energy portion of the density of states.

Finally, we would like to address an interesting problem, connected to the dynamics of quantum liquids and concerning the connection between the solid-phase density of states, $Z(\omega)$, and the corresponding quantity for liquids, namely the power spectrum of the velocity autocorrelation function (see for example Ref. [41]). We have already attempted to study this problem [25] using our previous low-energy spectral data of liquid para-hydrogen. However, for that case both temperature and density were changing and we could not go beyond a semi-quantitative interpretation of the spectra. We are confident that the present data, collected at constant temperature, could add useful information to this interesting problem. Work is in progress in this direction.

References

1. U. Balucani, M. Zoppi, *Dynamics of the liquid state* (Oxford University Press, Oxford, 1994).
2. S.W. Lovesey, *Theory of Neutron Scattering from Condensed Matter* (Clarendon Press, Oxford, 1987).
3. H.R. Glyde, *Excitations in liquid and solid helium* (Oxford Science Publications, Oxford, 1994).
4. G.I. Watson, J. Phys. Cond. Matt. **8**, 5955 (1999).
5. K.W. Herwig, P.E. Sokol, T.R. Sosnick, W.M. Snow, R.C. Blasdell, Phys. Rev. B **41**, 103 (1990).
6. C. Andreani, F. Filabozzi, M. Nardone, F.P. Ricci, J. Mayers, Phys. Rev. B **54**, 12744 (1994).
7. U. Bafile, M. Zoppi, F. Barocchi, R. Magli, J. Mayers, Phys. Rev. Lett. **75**, 1957 (1995).
8. U. Bafile, M. Zoppi, F. Barocchi, R. Magli, J. Mayers, Phys. Rev. B **54**, 11969 (1996).
9. D.M. Ceperley, R.O. Simmons, R.C. Blasdell, Phys. Rev. Lett. **77**, 115 (1996).
10. F. Albergamo, M. Nardone, A. Filabozzi, Phys. Rev. B **56**, 14614 (1997).
11. M. Celli, M. Zoppi, J. Mayers, Phys. Rev. B **58**, 242 (1998).
12. R.C. Blasdell, D.M. Ceperley, R.O. Simmons, Z. Naturforsh. **48a**, 433, (1993).
13. W. Langel, D.L. Price, R.O. Simmons, P.E. Sokol, Phys. Rev. B **38**, 11275 (1988).
14. K.W. Herwig, J.L. Gavilano, M.C. Schmidt, R.O. Simmons, Phys. Rev. B **41**, 96 (1990).
15. M. Zoppi, M. Neumann, Phys. Rev. B **43**, 10242 (1991).
16. U. Bafile, M. Zoppi, M. Celli, R. Magli, A.C. Evans, J. Mayers, Physica B **217**, 50 (1996).
17. J. Mayers, Phys. Rev. Lett. **71**, 1553 (1993).
18. Z.A. Bowden, M. Celli, F. Cilloco, D. Colognesi, R.J. Newport, S.F. Parker, F.P. Ricci, V. Rossi-Albertini, F. Sacchetti, J. Tomkinson, M. Zoppi, Physica B **276-278**, 98 (2000).
19. M. Zoppi, D. Colognesi, M. Celli, Eur. Phys. J. B **14**, 239 (2000).
20. C. Andreani, D. Colognesi, A. Filabozzi, M. Nardone, R.T. Azuah, Europhys. Lett. **37**, 329 (1997).
21. R.D. McCarty, J. Hord, H.M. Roder, *Selected Properties of Hydrogen*, NBS Monograph **168**, (1981).
22. R.L. Mills, J. Low Temp. Phys. **31**, 423 (1977).
23. I.F. Silvera, A. Driessen, J.A. de Waal, Phys. Lett. A **68**, 207 (1978).
24. I.F. Silvera, Rev. Mod. Phys. **52**, 393 (1980).
25. M. Zoppi, D. Colognesi, M. Celli, Europhys. Lett. **53**, 34 (2001).
26. V.F. Sears, Phys. Rev. B **30**, 44 (1984).
27. M. Moraldi, M. Santoro, L. Ulivi, M. Zoppi, Phys. Rev. B **58**, 234 (1998).
28. V.F. Sears, Can. J. Phys. **63**, 68 (1985).
29. J. Schaefer, W.E. Köhler, Z. Phys. D **13**, 217 (1989).
30. I.F. Silvera, V.V. Goldman, J. Chem. Phys. **69**, 4209 (1978).
31. Q. Wang, J.K. Johnson, J.Q. Broughton, Mol. Phys. **89**, 1105 (1996).
32. D.C. Wallace, *Thermodynamics of Crystals* (Wiley, New York, 1972).
33. V.S. Vorob'ev, Sov. Phys. JETP **82**, 85 (1996).
34. M. Nielsen, Phys. Rev. B **7**, 1626 (1973).
35. J.K. Krause, C.A. Swenson, Phys. Rev. B **21**, 2533 (1980).
36. A. Bickermann, H. Spitzer, H. Stiller, H. Meyer, R.E. Lechner, F.Volino, Z. Phys. B **31**, 345 (1978).
37. B.A. Vindryaevskii, S.N. Ishmaev, G.V. Kobelev, I.P. Sadikov, V.A. Sukhoparov, A.S. Telepnev, A.A. Chernyshov, Sov. J. Low Temp. Phys. **15**, 258 (1989).
38. J.A. Young, J.U. Koppel, Phys. Rev. A **135**, 603 (1964).
39. M. Celli, D. Colognesi, M. Neumann, M. Zoppi, work in progress (2001).
40. B.A. Vindryaevskii, S.N. Ishmaev, I.P. Sadikov, A.A. Chernyshev, Yu.L. Shitikov, G.V. Kobelev, V.A. Sukhoparov, A.S. Telepnev, JETP Lett. **62**, 822 (1995).
41. A. Rahman, K.S. Singwi, A. Sjölander, Phys. Rev. **126**, 986 (1962).